Published in final edited form as:
Nat Cell Biol. 2004 January ; 6(1): 21–30. doi:10.1038/ncb1075.

Mammalian formin-1 participates in adherens junctions and polymerization of linear actin cables

Agnieszka Kobielak, **H. Amalia Pasolli**, and **Elaine Fuchs**
Howard Hughes Medical Institute, Laboratory of Mammalian Cell Biology and Development, The Rockefeller University, 1230 York Avenue, Box 300, New York, NY 10021-6399, USA.

Abstract

During epithelial sheet formation, linear actin cables assemble at nascent adherens junctions. This process requires α-catenin and actin polymerization, although the underlying mechanism is poorly understood. Here, we show that formin-1 interacts with α-catenin, localizes to adherens junctions and nucleates unbranched actin filaments. Furthermore, disruption of the α-catenin–formin-1 interaction blocks assembly of radial actin cables and perturbs intercellular adhesion. A fusion protein of the β-catenin-binding domain of α-catenin with the actin polymerization domains of formin-1 rescues formation of adherens junctions and associated actin cables in *α-catenin*-null keratinocytes. These findings provide new insight into how α-catenin orchestrates actin dynamics during intercellular junction formation.

The actin cytoskeleton is critical for many cellular processes, including migration, polarization, cytokinesis and adhesion. Actin filaments are polar structures, possessing a fast-growing 'barbed' end that is regulated through an inhibitory cap[1]. Uncapping the barbed end or severing F-actin to generate a new barbed end can stimulate filament elongation. Actin polymerization can also occur *de novo* through rate-limiting nucleation events.

Branched actin networks containing short filaments are nucleated through activation of the conserved Arp2/3 complex, which functions broadly across eukaryotes[2-5]. Such networks are prevalent in lamellipodia and other regions where spreading and migration are important. In contrast, nucleation of unbranched actin cables involves formins[6-11]. Key to this process are two formin-homology (FH) domains that modulate F-actin assembly: an actin polymerization domain (FH2) and a proline-rich domain to recruit profilin-bound G-actin (FH1). Although most formins possess these conserved domains, their functionality has only been demonstrated directly for yeast formins and for a murine cousin, mDia1, which belongs to the Diaphanous subfamily of formins[6-11]. Given the diverse functions attributed to different mammalian formins[12-20], an as yet unresolved issue is whether this diversity arises from differences in their ability to polymerize actin, or to localize and/or regulate actin polymerization.

In mammalian epithelia, both branched actin networks and linear actin cables are involved in intercellular adhesion[21-24].During the initial phases, activated Rho GTPases stimulate lamellipodial (branched F-actin) and filopodial (F-actin cable) extensions[25-27]. Once nascent junctions (puncta) have assembled from clusters of transmembrane E-cadherins, β-catenin and α-catenin, contacts are stabilized by attachment and assembly of a linear, radial actin cable at

Correspondence should be addressed to: E.F. (e-mail: fuchslb@rockefeller.edu)..

Note: Supplementary Information is available on the Nature Cell Biology website.

COMPETING FINANCIAL INTERESTS
The authors declare that they have no competing financial interests.

the tip of each puncta[21-23]. Through interactions with adherens junctions, the actin cytoskeleton can polarize and seal membranes into a sheet of adhering epithelial cells[21-24].

Although puncta are sites of active actin polymerization[23], it is not clear how the radial actin cable assembles.Vasp and Mena proteins localize to puncta and are necessary for cell–cell adhesion[23], and although they do not nucleate actin polymerization, they elongate pre-existing F-actin by competing with inhibitory cap proteins for barbed ends[28]. Arp2/3 binds E-cadherin and could be involved in actin dynamics at puncta[29], but the linear nature of radial actin cables seems more compatible with behaviour attributed to formins. Although experiments with mutant forms of mDia1 suggest a potential role for formins[30], endogenous formins have not been localized to sites of cell–cell adhesion. Whatever the underlying mechanism, conditional gene targeting studies identified an essential role for α-catenin in radial actin cable formation and in stabilizing adherens junctions to assemble epithelial sheets[23,31].

Here, we used the yeast two-hybrid system to analyse in more detail the mechanism governing radial actin cable formation at adherens junctions. We identify and characterize formin-1, the founding member of the formin superfamily[13], as a novel binding partner for α-catenin. In addition,we demonstrate that formin-1 can nucleate the polymerization of unbranched actin filaments *in vitro* and can function *in vivo* in α-catenin-dependent, radial actin cable formation.

RESULTS

Formin-1 interacts with α-catenin

To preserve the tertiary structure of α-catenin[2-35], a yeast two-hybrid screen of newborn mouse skin cDNAs was performed using full-length α-catenin cDNA as bait. Previously known interaction partners, including β-catenin and plakoglobin, were identified (Fig. 1a). In addition, two independent clones encoding formin1 gene products were identified. *Formin-1* is known to be mutated in limb deformity (*ld/ld*) mutant mice[36-38].

One of the two clones encoded sequences previously reported in the formin-1 isoform, formin-1 (IV)[39] (amino acids 453–600; Fig. 1b). The other encoded a segment (amino acids 8–262) of a novel isoform, formin-1 (V). Both formins interacted with α-catenin irrespective of which was used as bait (linked to the Gal4 binding domain; BD) and which was screened (linked to the Gal4 activation domain; AD; Fig. 1a, shown are data for bait). RT–PCR confirmed the presence of formin-1 (I), (IV) and (V) mRNAs (Fig. 1c), but not formin-1 (II) and (III) mRNAs (data not shown), in skin and cultured keratinocytes. Northern blot analyses identified formin-1 (IV) as the most abundant isoform in keratinocytes, as it is in limb bud ectoderm[38]. As formin-1 (V) represents a novel isoform, the transcript was isolated and characterized. Unique amongst the formin isoforms, formin-1 (V) contains an in-frame start codon within exon 3. Thereafter, it is identical to formin-1 (Ib), which possesses exons 5, 7–16 and 18–24 (ref. 38).

All of these isoforms possess exons encoding the FH1 (exon 9) and FH2 (exons 13–16 and 18) domains required for nucleating actin polymerization (Fig. 1b)[20]. Formin-1 (IV) differs from formin-1 (V) in that the coding sequence starts within and encompasses exon 6, which contains the FH3 domain, part of which may be involved in regulating formin activity[20]. Taken together, these data extend the expression pattern of formin-1 (IV) mRNA to skin, identify a novel formin-1 mRNA and provide a potential link to α-catenin, which might be relevant in understanding its essential role in actin cable formation.

Formin-1 localizes to adherens junctions in an α-catenin-dependent manner

To address whether the formin-1–α-catenin association is physiologically relevant, immunofluorescence microscopy was performed on skin from wild-type mice and mice conditionally null for α-catenin (Fig. 2)[31]. Staining with an anti-formin-1 (IV) antibody

identified formin-1 in both the dermis and epidermis (Fig. 2a, a′). In epidermis, formin-1 localized to the cytoplasm and to cell–cell borders. Significantly, the localization of formin-1 to cell–cell borders was perturbed in *α-catenin*-null epidermis (Fig. 2b, b′). In cultured wild-type keratinocytes, formin-1 antibodies exhibited a distinctive punctate staining at developing cell–cell contacts (Fig. 2c). Punctae were characteristic of nascent adherens junctions[23] and colocalized with staining for α-catenin (data not shown) and vinculin. Anti-formin-1 also labelled F-actin bundles radiating from punctae (Figs 2d, j). At later stages, anti-formin-1 localized along cell–cell borders (Figs 2e, k), typical of the linear staining patterns of antibodies against classical adherens junction proteins.

In the absence of α-catenin, keratinocytes exhibited few cell–cell junctions or radial actin cables, as revealed by antibodies against formin-1 (IV) or adherens junction proteins (Fig. 2f-h)[23]. Even densely plated α-catenin knockout cultures treated with calcium for 24 h failed to undergo actin organization and lacked cell–cell border labelling (Fig. 2h). These aberrations in formin organization seemed to be selective, as the overall actin cytoskeleton was still largely intact (Fig. 2l-n). Thus, there is a distinct correlation between the presence of α-catenin at adhesion zippers, the formation of radial actin cables and the localization of formin-1 at these sites.

Specific domains of formin-1 and α-catenin are necessary for epidermal sheet formation

Co-immunoprecipitation analysis was used to address whether formin-1 and α-catenin associate directly, and to further define the interaction (Fig. 3). The cytomegalovirus (CMV) promoter was used to drive transient expression of c-Myc-tagged α-catenin and Flag-tagged formin-1 in COS epithelial cells. Both ΔC-formin-1 (IV) and ΔC-formin-1 (V) formed a complex with α-catenin that could be immunoprecipitated with antibodies against the Flag or c-Myc epitopes (Fig. 3a). A 142-amino-acid overlap between these interacting segments defined the α-catenin-binding domain (α-cat-BD). This site encompasses the coiled-coil domain between the FH3 and FH1 domains, is present in isoforms Ia, Ib, IV and V, and is sufficient to maintain the formin-1–α-catenin interaction.

To assess whether the formin-1–α-catenin interaction occurs at cell–cell junctions, GFP–formin-1-cc (α-cat-BD) was expressed in wild-type and *α-catenin*-null keratinocytes (Fig. 3b). This fragment localized to cell borders only in the presence of elevated calcium (for 24 h) and α-catenin. Immunoprecipitation analysis verified that this interaction also occurs between full-length formin-1 isoforms found naturally in epidermal keratinocytes. Anti-α-catenin coprecipitated endogenous formin-1 (IV), as demonstrated by western blotting with an anti-formin-1 (IV)-specific antibody (Fig. 3d). Coprecipitation was dependent on the presence of endogenous α-catenin, as formin-1 (IV) was not detected in *α-catenin*-null lysates.

To define the formin-1-binding site of α-catenin, we engineered a series of Myc-tagged vectors that each encode a known structural domain of α-catenin[32-35] (Fig. 3c). Each construct was transiently co-expressed with Flag-tagged ΔC-formin-1 (IV) in COS cells before anti-Myc immunoprecipitation and anti-Flag western blotting. Of the five major domains, only the vinculin/α-actinin-binding site (amino acids 300–500) exhibited specific interactions with ΔC-formin-1 (IV) (Fig. 3c).

Formin-1 nucleates polymerization of unbranched actin filaments

To assess whether formin-1 participates in the polymerization and formation of radial actin cables at nascent junctions, we first tested whether formin-1 stimulates unbranched F-actin assembly *in vitro*. Five glutathione *S*-transferase (GST) fusion proteins were generated and purified (Fig. 4a): Formin-1 (FH1-FH2) encompasses the carboxy-terminal FH1 and FH2 domains common to all isoforms; formin-1 (Ld-mut) is similar to formin-1 (FH1-FH2), except

that it is C-terminally truncated to reflect a severe *formin-1* mutation found in *limb deformity* mutant mice (ref. 38); formin-1 (ΔFH2) completely lacks the FH2 domain; ΔC-formin-1 (IV) encompasses the FH3 domain and the α-catenin-binding (coiled-coil, cc) domain; α-cat contains the full length α-catenin coding sequence. Western blot analyses enabled quantification of protein concentration and verified that the proteins were stable and of the predicted size (Fig. 4b).

Varying amounts (10–200 nM) of formin-1 (FH1-FH2) were exposed to 4 μM purified actin[1]. A fluorimeter was then used to measure the increase in pyrene-conjugated actin (10% of pyrene–G-actin) that occurs as a result of polymerization. Formin-1 (FH1-FH2) enhanced the rate of actin polymerization markedly over that which occurs spontaneously under these conditions (Fig. 4c). The polymerizing activity of the formin-1 FH1-FH2 C-terminal segment was dose-dependent (Fig. 4c), and its ability to stimulate polymerization increased with initial G-actin concentration (Fig. 4d).

A role for formin-1 (FH1-FH2) in barbed-end filament growth was strengthened by further observations. First, treatment with 200 nM formin-1 (FH1-FH2) inhibited barbed-end depolymerization when F-actin was diluted to 0.1 μM; that is, below the critical concentration required for polymerization at the barbed end[40] (Fig. 4e). Moreover, the protective features of formin-1 were concentration-dependent. Second, treatment with cytochalasin D, an inhibitor of barbed-end growth[41], reduced the stimulatory effects of formin-1 (FH1-FH2) (Fig. 4f). In contrast, profilin, which blocks spontaneous nucleation and specifically inhibits pointed-end growth[10], only reduced formin-1 (FH1-FH2) nucleation by ~10% (Fig. 4f). The ability of formin-1 to utilize profilin-bound G-actin suggests that it can enhance F-actin polymerization under physiological conditions.

Interestingly, formin-1 (Ld mut) stimulated F-actin polymerization *in vitro* (Fig. 4f). By this criterion, the *ld/ld* phenotype in mice seems to be caused by defects that go beyond the ability of formin-1 to stimulate actin polymerization. Removal of the entire FH2 domain abolished the stimulatory effects of formin-1 (Fig. 4f), as previously observed for yeast formin FH2 (refs 6, 8, 10 and 11). The effects of formin-1 seemed to be specific for nucleation, rather than elongation, as pre-polymerized filaments seemed to be unaffected by formin-1 (data not shown).

Diaphanous formins contain self-interacting domains within their N- and C-terminal segments[11]. In this regard, it is interesting that ΔC-formin-1 (IV) inhibited the actin nucleation activity of formin-1 (FH1-FH2) (Fig. 4f). Additionally, co-immunoprecipitation analysis suggested that the N- and C-terminal domains of formin-1 (IV) interact (data not shown). In contrast, the distinctive N-terminal segment of formin-1 (V) did not exhibit N–C-terminal associations or inhibit F-actin under these conditions. α-Catenin did not rescue the negative effects of ΔC-formin-1 (IV) on actin assembly (Fig. 4f), indicating that α-catenin itself does not mediate this autoregulation. Whether Rho GTPases are involved in the underlying mechanism is unknown, although they regulate the process in other formins and have also been implicated in adherens junction formation[11,21-27].

To evaluate further the effects of formin-1 (FH1-FH2) on nucleation of F-actin assembly and to assess its ability to promote linear actin cable formation, we used fluorescence and electron microscopy to examine the actin polymers produced in the presence and absence of profilin and formin-1. In the absence of formin-1, 4 μM actin yielded a small number of long filaments (18 ± 0.5 μm) after exposure to polymerization buffer for 10 min (Fig. 4g). In contrast, addition of 20–100 nM formin-1 resulted in >15-fold increase in the number of filaments, which on average were shorter (2 ± 0.2 μm; Fig. 4h, i). Filament numbers increased in a dose-dependent manner as the concentration of formin-1 (FH1-FH2) increased, supporting a role in nucleation.

Addition of profilin increased polymer length (4 ± 0.5μm), in support of barbed-end polymerization (Fig. 4j). Notably, actin polymers were ~8 nm (typical for uranyl acetate staining) and unbranched (Fig. 4k, l). Taken together, these results provide compelling evidence that formin-1 can nucleate the assembly of linear F-actin.

Formin-1α-cat-BD disrupts radial actin cable assembly at nascent cell–cell junctions

To further examine the role of formin-1 on the actin dynamics required for adherens junction formation, we overexpressed a green fluorescent protein (GFP)–ΔC-formin-1 (IV) fusion protein, which encompasses α-cat-BD, but lacks FH1-FH2 (Fig. 5a). As a negative control, we generated ΔC-Δcc-formin-1 (IV), a mutant similarly truncated at the C terminus but which lacks α-cat-BD. To check for formin specificity, ΔC-mDia1 was used, which contains the FH3 and coiled-coiled segments of the Diaphanous formin, mDia1 (ref. 30). In contrast to ΔC-formin-1 (IV), ΔC-mDia1 did not form a complex with Myc–α-catenin when expressed at comparable levels in COS cells (Fig. 5b). Additionally, the sequence identity between α-cat-BD from formin-1 (IV) and the corresponding segment of mDia1 was only 19%.

Epidermal sheets of primary keratinocytes are polarized, with apical honeycomb-like cell–cell junctions (see Fig. 2e, k, for example). Transient expression of ΔC-formin-1 (IV) in keratinocytes allowed visualization of this architecture by epifluorescence microscopy. Wherever both neighbouring cells expressed this ΔC-formin-1 (IV), cell–cell junctions were markedly and specifically disrupted at the border (Fig. 5c, d). Addition of an anti-formin-1 antibody or antibodies against known adherens junction markers, including β-catenin, α-catenin, vinculin and Vasp, failed to localize to the shared borders of these non-adhering cells (data not shown). In contrast, cell–cell adhesion between a transfected and untransfected cell seemed to be unperturbed (Fig. 5c; irregularities at some cell–cell borders reflect extensive lamellipodial ruffling in these cultures[11]).

Phalloidin labelling revealed an intact actin cytoskeleton in most transfected cells exposed to ΔC-formin-1 (IV) (Fig. 5d), and is consistent with the lack of profilin and actin polymerization domains in this mutant. Notably, however, at earlier times during adhesion, radial actin cables were often perturbed at the cell–cell junctions of two transfected cells (data not shown). In cases where only one cell was transfected, puncta and radial actin cables were restricted to the untransfected cell of the pair (Fig. 5e, see inset).

The behaviour of mixtures of wild-type and ΔC-formin-1 (IV)-expressing cells was strikingly similar to that observed with mixtures of wild-type and *α-catenin*-null keratinocytes[23]. In both cases, the effects on the actin network seemed to be selective rather than global. Moreover, the perturbations caused by ΔC-formin-1 (IV) were dependent on its ability to interact with α-catenin. Thus, cells that expressed ΔC-Δcc-formin-1 (IV) still exhibited cell–cell border staining with an anti-E-cadherin antibody (Fig. 5f, g) and still displayed radial actin cables at puncta (Fig. 5h). Similarly, overexpression of ΔC-mDia1 did not affect the junctional localization of E-cadherin and α-catenin (Fig. 5i, j), and radial actin cables still formed in these transfected cells (Fig. 5k).

Overall, these findings suggest that: first, ΔC-formin-1 (IV) contains an α-catenin-binding domain that is not conserved in its cousin mDia1; second, this domain disrupts cell–cell junction formation by perturbing the assembly of radial actin cables at nascent adherens junctions, rather than by gross perturbations of the actin cytoskeleton. The data support our earlier finding that radial actin cables at one of two sides of an adhesion zipper are sufficient to form cell–cell junctions and epithelial sheets[23].

If the ability of α-catenin to recruit formin-1 is key to orchestrating actin dynamics during adherens junction formation, then recruitment of the formin-1 FH1-FH2 C-terminal domain to

E-cadherin–β-catenin complexes might rescue cell–cell junction formation in *α-catenin*-null keratinocytes. To test this possibility, we constructed GFP–β-cat-BD–(FH1-FH2). For this experiment, three additional GFP-tagged proteins were also engineered as controls: full-length α-catenin, FH1-FH2 and β-cat-BD (FH1) (Fig. 6a). Anti-GFP western blotting confirmed that the expressed proteins were stable and migrated at the predicted size (Fig. 6b, left). When expressed in keratinocytes, β-cat-BD (FH1-FH2) and β-cat-BD (FH1) co-immunoprecipitated with anti-β-catenin (Fig. 6b, right).

As noted previously[23], *α-catenin*-null keratinocytes yield only small infrequent patches of anti-E-cadherin staining at cell borders (Fig. 6c, arrows), even after 24 h in high-calcium medium. However, when α-catenin–GFP was expressed, lines of anti-E-cadherin were observed between neighbouring cells (Fig. 6d). GFP–α-catenin also rescued radial actin cable formation at earlier times after the calcium switch (data not shown).

In contrast to α-catenin, the actin polymerization (FH1-FH2) domains of formin did not rescue formation of nascent adherens junctions, radial actin cables or epithelial sheets (Fig. 6e, f). This was true even when cells made direct contact with one another and when both cells expressed the transgene (compare Fig. 6f with 6d). Interestingly, however, these features could be rescued by comparable expression of β-cat-BD (FH1-FH2), which targeted formin-1 actin polymerization domains to developing adherens junctions (Fig. 6g, h). Although the rescues were not complete, they were significant given that they occurred in transiently transfected cells and in the absence of α-catenin. Moreover, efficient rescue was dependent on the actin polymerization domain, as judged by the marked difference in cell–cell border localization of anti-E-cadherin in keratinocytes transfected with β-cat-BD (FH1) (Fig. 6i).

In wild-type, but not *α-catenin*-null, keratinocytes, Vasp and Mena localized to E-cadherin-mediated cell–cell junctions[23] (Fig. 6j, k). Notably, in β-cat-BD (FH1-FH2)-transfected *α-catenin*-null cells, an anti-Vasp antibody labelled cell–cell borders (Fig. 6l). As α-catenin was absent, this finding identifies an ability of formin-1 to localize Vasp to cell–cell junctions. Whether this association is direct or indirect, and whether it is exclusively governed by formin-1, are intriguing questions beyond the scope of this study.

Finally, whereas the morphology seemed unchanged in the brightest GFP–β-cat-BD (FH1)-expressing knockout cells, the brightest GFP–β-cat (FH1-FH2)- and GFP–(FH1-FH2)-expressing knockout cells often extended exaggerated membrane protrusions and displayed dense actin networks (data not shown). Overexpression of other constitutively activated formins has been shown to have similar effects[7,20].

DISCUSSION

Although yeast formins and their closest mouse homologue, mDia1 (30–40% identical), have recently been shown to induce actin polymerization through their FH1 and FH2 domains, comparable studies have not yet been reported for other formins, which now constitutes a large (at least 9) multigene family in mammals.

The fact that formin-1 is stimulatory for actin polymerization is particularly striking, given that it is encoded by *formin-1*, a gene that is disrupted in the *limb deformity* mutant mouse[36-38]. It was originally surmised that formin-1 might function in a regulatory Shh–FGF (sonic hedgehog–fibroblast growth factor) feedback loop necessary for apical ectodermal ridge formation and that its function was compromized in the *ld/ld* mutant mice[12,13]. Recently, however, it was discovered that *gremlin*, a gene adjacent to the *formin-1* locus that is downregulated in *limb deformity* mice, encodes a BMP antagonist essential for the maintenance of Shh and FGF signalling during limb patterning[42]. This raises the possibility that the major *ld/ld* phenotype may not reflect loss of formin-1 function. Our findings suggest that the primary

function of formin-1 may be to regulate actin polymerization, a function that has not been reported previously.

An important question is whether other formins share formin-1 functions, particularly in epithelial sheet formation. Although mDia1 has not been localized to adherens junctions, a role for mDia1 at these sites has been postulated from the ability of a 440-amino-acid truncated form of mDia1 (encompassing much of the conserved FH1 and FH2 domains) to impair cytokinesis and disrupt cell–cell adhesion. In this case, intercellular adhesion was disrupted between single transfected epithelial cells and their wild-type neighbours[30]. Such effects go beyond (and may not involve) radial actin cable assembly, which must be compromised on both sides of a junction to disrupt intercellular contacts[23]. Additionally, and in contrast to formin-1, the FH3-coiled coil domain of mDia1 (ΔC-mDia1) did not bind α-catenin nor perturb radial actin cable formation. A similar construct, mDia-ΔRBD-ΔC, also had no effect on MDCK epithelial adhesion[43]. Thus, if mDia1 is involved in adherens-junction-mediated radial actin cable formation, it is likely to differ in the manner through which it associates with junctional components.

An intriguing and distinctive feature of diaphanous formins is their autoregulation[20,44-46]. The Rho GTPase-binding domain (RBD) for this formin subfamily maps to a sequence that overlaps with, and is N-terminal to, FH3 (refs 20, [46-48]). A C-terminal diaphanous auto-inhibitory domain (DAD) maintains the formin in a dormant state until activated Rho GTPase binds and relieves auto-inhibition, and nucleates localized actin assembly[11,46,49]. Interestingly, the N- and C-terminal segments of formin-1 (IV) interact, and this interaction impairs actin polymerization. Moreover, α-catenin does not disrupt this interaction *in vitro*, suggesting that other factors may be required to unleash the actin-polymerizing potential of formin-1 (IV). When coupled with the well-established involvement of Rho GTPases and dynamic actin rearrangements in epithelial sheet formation[27,50], the potential link between formin-1 (IV) and these actin regulatory proteins merits further investigation. An attractive model consistent with our findings is that in conjunction with Rho GTPases, α-catenin recruits formin-1 to nucleate profilin-mediated F-actin assembly at puncta. Vasp may then compete with the capping protein to promote extension of these initiated, unbranched, F-actin structures to form linear, radial actin cables and to seal epithelial sheets.

METHODS

Plasmid construction

Details of plasmids can be found in Supplementary Information, Table 1. All cloned fragments were sequenced in their entirety. Pfu polymerase (Stratagene, La Jolla, CA) was used to amplify full-length mouse formin-1 (I, IV and V) sequences from mouse keratinocyte cDNA. Constructs were tagged with Flag, Myc, GFP or GST by cloning the cDNAs inframe into pCMV-Tag-4A, pCMV-Tag-5A (Stratagene), pCMV-EGFP-C1 (Clontech, Palo Alto, CA) or pGEX-4T vectors (Amersham Pharmacia, Piscataway, NJ), respectively.

Yeast two-hybrid analysis

The Matchmaker two-hybrid system 3 (Clontech) was employed as recommended by the manufacturer. An *Eco*RI fragment encompassing the full-length murine α-catenin cDNA was cloned into the yeast pGBKT7 plasmid (Clontech). The GAL4-BD–α-catenin fusion protein was non-toxic and did not induce autonomous activation. This bait was then used in Y190 yeast cells to screen a directionally cloned mouse newborn skin cDNA library prepared in the pGAD yeast expression vector, which generates GAL4-activating domain (AD)–cDNA fusion products (Clontech). Co-transformants were plated in −Leu, −Trp, −His medium to screen for interacting proteins. Colonies were then subjected to additional selection first in −Leu, −Trp,

−His, −Ade medium (8 days), and then by testing for *lacZ* expression as judged by a Galacto-Light Plus chemiluminescent reporter (Tropix, Bedford, MA) assay. From these positive clones, AD–library plasmid DNAs were then isolated and retransformed with empty vector (control) and bait (test) to confirm their interaction with α-catenin.

Immunoprecipitation and western blotting

Protein extracts were prepared as described[23]. Agarose-bead-conjugated anti-Myc (Clontech) or affinity gel-conjugated anti-Flag M2 (Sigma, St Louis, MO) antibodies were incubated with extracts for 12 h at 4 °C. Alternatively, extracts were pre-incubated with Protein G–Sepharose (Amersham, Pharmacia) for 1 h at 4 °C before addition of the appropriate antibody for 3 h. All precipitates were washed three times with lysis buffer before SDS–PAGE, immunoblotting and visualization by chemiluminescence.

Protein purifications

BL21 tuner strains (Amersham Pharmacia) were transformed with plasmids encoding GST–formin-1. IPTG (1 mM) was used to induce plasmid expression according to the manufacturer's suggestions. Cultures were resuspended in extraction buffer (1.4 M NaCl, 100 mM Na_2HPO_4, 18 mM KH_2PO_4 at pH 7.5) with protease inhibitor cocktail and 5 mM dithiothreitol. After sonication and high-speed centrifugation, supernatants were incubated with glutathione–Sepharose before washing and elution in 50 mM glutathione. Solutions were dialysed against HEK buffer (20 mM Hepes at pH 7.5, 1 mM EDTA, 50 mM KCl, 5% glycerol and 5 mM DTT), concentrated with CentriPrep YM-100 and YM-60 units (Amicon, Bedford, MA) and flash frozen in liquid nitrogen.

Pyrene–actin polymerization assays

10% pyrene-labelled rabbit muscle actin (Cytoskeleton, Denver, CO) in G-buffer (0.02 mM $CaCl_2$, 0.5 mM Tris-HCl at pH 8.0 and 0.02 mM ATP) was centrifuged at 150,000*g* for 30 min before use to remove any polymerized material/debris. Pyrene–actin (0–4 μM) was then combined with 10–200 nM formin-1-derived constructs in G buffer. Polymerization was induced by addition of actin polymerization buffer (12.5 mM KCl, 0.5 mM $MgCl_2$ and 0.025 mM ATP) and pyrene fluorescence was monitored with a PolarStar (BMG) fluorimeter (Oftenburg, Germany; excitation at 365 nm, emission at 407 nm).

For the actin depolymerization assay, pre-assembled actin filaments were incubated with formin-1-derived constructs or treated with cytochalasin D for 5 min. Depolymerization was induced by dilution in F-buffer (G-buffer containing 1× actin polymerization buffer) and pyrene fluorescence was monitored. Inhibition of F-actin elongation with cytochalasin D was assessed by observing pyrene fluorescence of 4 μM actin (10% pyrene-labelled) combined with GST–formin-1-FH1-FH2 (200 nM) ± 100nM cytochalasin D in polymerization buffer.

For epifluorescence microscopy of F-actin, polymerization products were labelled with rhodamine–phalloidin (Sigma)[10], applied to coverslips coated with poly-L-lysine and analysed (Axiovert 200M; Zeiss, Thornwood, NY). For ultrastructural analysis, aliquots from the reaction were spotted onto carbon- and formvar-coated grids, negatively stained with 1% aqueous uranyl acetate and examined at 80 kV on a Tecnai G2 12 transmission electron microscope (Hillsboro, OR).

Preparation of primary keratinocytes

Primary keratinocytes were cultured from newborn mouse skin as described previously[23].Cells were seeded on glass coverslips with grid (Eppendorf, Hamburg, Germany) or permanox slides coated with poly-L-lysine, collagen I and fibronectin. After 24 h, attached cells were transfected

with Fugene (Roche). After a further 24 h, adherens junction formation was induced by increasing the $CaCl_2$ concentration from 0.05 mM to 2 mM for either 2.5–8 h (puncta) or 24 h (epithelial sheet formation), followed by fixation and staining.

Immunofluorescence microscopy

Cells were fixed in 4% formaldehyde/PBS for 10 min before double indirect immunostaining[23] and viewing with an Axiovert 200M microscope (Zeiss) or LSM 510 confocal microscope (Zeiss). Primary antibodies used were raised against E-cadherin (Zymed, San Francisco, CA), β-catenin, α-catenin, vinculin, α-actinin (Sigma), Vasp (M4; Alexis, San Diego, CA) and formin IV (a gift from L. Cantley, Yale University, School of Medicine). Phalloidin–TRITC (Sigma) was used to visualize filamentous actin. Unless stated, dilutions were according to the manufacturer's recommendations. Fluorescently conjugated secondary antibodies were from ImmunoResearch (West Grove, PA).

Supplementary Material

Refer to Web version on PubMed Central for supplementary material.

ACKNOWLEDGEMENTS

E.F. is an investigator of the Howard Hughes Medical Institute. We thank V. Vasioukhin for valuable discussions in the early stages of this work, W. Lowry for assistance with the actin polymerization studies, A. North and A. Vaezi for their assistance with Deltavision imaging, and P. Leder, A. Alberts, S. Narumiya and L. Cantley for reagents. This work was supported by the National Institutes of Health (RO1-AR27883 to E. F.) and the Howard Hughes Medical Institute.

References

1. Pollard TD, Blanchoin L, Mullins RD. Molecular mechanisms controlling actin filament dynamics in nonmuscle cells. Annu. Rev. Biophys. Biomol. Struct 2000;29:545–576. [PubMed: 10940259]
2. Mullins RD, Stafford WF, Pollard TD. Structure, subunit topology, and actin-binding activity of the Arp2/3 complex from *Acanthamoeba*. J. Cell Biol 1997;136:331–343. [PubMed: 9015304]
3. Welch MD, Rosenblatt J, Skoble J, Portnoy DA, Mitchison TJ. Interaction of human Arp2/3 complex and the *Listeria monocytogenes* ActA protein in actin filament nucleation. Science 1998;281:105–108. [PubMed: 9651243]
4. Winter DC, Choe EY, Li R. Genetic dissection of the budding yeast Arp2/3 complex: a comparison of the *in vivo* and structural roles of individual subunits. Proc. Natl Acad. Sci. USA 1999;96:7288–7293. [PubMed: 10377407]
5. Welch MD, Mullins RD. Cellular control of actin nucleation. Annu. Rev. Cell Dev. Biol 2002;18:247–288. [PubMed: 12142287]
6. Pruyne D, et al. Role of formins in actin assembly: nucleation and barbed-end association. Science 2002;297:612–615. [PubMed: 12052901]
7. Sagot I, Klee SK, Pellman D. Yeast formins regulate cell polarity by controlling the assembly of actin cables. Nature Cell Biol 2002;4:42–50. [PubMed: 11740491]
8. Sagot I, Rodal AA, Moseley J, Goode BL, Pellman D. An actin nucleation mechanism mediated by Bni1 and profilin. Nature Cell Biol 2002;4:626–631. [PubMed: 12134165]
9. Evangelista M, Pruyne D, Amberg DC, Boone C, Bretscher A. Formins direct Arp2/3-independent actin filament assembly to polarize cell growth in yeast. Nature Cell Biol 2002;4:260–269. [PubMed: 11875440]
10. Kovar DR, Kuhn JR, Tichy AL, Pollard TD. The fission yeast cytokinesis formin Cdc12p is a barbed end actin filament capping protein gated by profilin. J. Cell Biol 2003;161:875–887. [PubMed: 12796476]
11. Li F, Higgs HN. The mouse formin mDia1 is a potent actin nucleation factor regulated by autoinhibition. Curr. Biol 2003;13:1335–1340. [PubMed: 12906795]

12. Chan DC, Wynshaw-Boris A, Leder P. Formin isoforms are differentially expressed in the mouse embryo and are required for normal expression of fgf-4 and shh in the limb bud. Development 1995;121:3151–3162. [PubMed: 7588050]
13. Zuniga A, Zeller R. Gli3 (Xt) and formin (ld) participate in the positioning of the polarising region and control of posterior limb-bud identity. Development 1999;126:13–21. [PubMed: 9834182]
14. Lee L, Klee SK, Evangelista M, Boone C, Pellman D. Control of mitotic spindle position by the Saccharomyces cerevisiae formin Bni1p. J. Cell Biol 1999;144:947–961. [PubMed: 10085293]
15. Heil-Chapdelaine RA, Adames NR, Cooper JA. Formin' the connection between microtubules and the cell cortex. J. Cell Biol 1999;144:809–811. [PubMed: 10085282]
16. Leader B, et al. Formin-2, polyploidy, hypofertility and positioning of the meiotic spindle in mouse oocytes. Nature Cell Biol 2002;4:921–928. [PubMed: 12447394]
17. Tolliday N, VerPlank L, Li R. Rho1 directs formin-mediated actin ring assembly during budding yeast cytokinesis. Curr. Biol 2002;12:1864–1870. [PubMed: 12419188]
18. Geneste O, Copeland JW, Treisman R. LIM kinase and Diaphanous cooperate to regulate serum response factor and actin dynamics. J. Cell Biol 2002;157:831–838. [PubMed: 12034774]
19. Lew DJ. Formin' actin filament bundles. Nature Cell Biol 2002;4:E29–E30. [PubMed: 11835051]
20. Wallar BJ, Alberts AS. The formins: active scaffolds that remodel the cytoskeleton. Trends Cell Biol 2003;13:435–446. [PubMed: 12888296]
21. Yonemura S, Itoh M, Nagafuchi A, Tsukita S. Cell-to-cell adherens junction formation and actin filament organization: similarities and differences between non-polarized fibroblasts and polarized epithelial cells. J. Cell Sci 1995;108:127–142. [PubMed: 7738090]
22. Adams CL, Chen YT, Smith SJ, Nelson WJ. Mechanisms of epithelial cell–cell adhesion and cell compaction revealed by high-resolution tracking of E-cadherin–green fluorescent protein. J. Cell Biol 1998;142:1105–1119. [PubMed: 9722621]
23. Vasioukhin V, Bauer C, Yin M, Fuchs E. Directed actin polymerization is the driving force for epithelial cell–cell adhesion. Cell 2000;100:209–219. [PubMed: 10660044]
24. Vaezi A, Bauer C, Vasioukhin V, Fuchs E. Actin cable dynamics and Rho/Rock orchestrate a polarized cytoskeletal architecture in the early steps of assembling a stratified epithelium. Dev. Cell 2002;3:367–381. [PubMed: 12361600]
25. Adams CL, Nelson WJ. Cytomechanics of cadherin-mediated cell–cell adhesion. Curr. Opin. Cell Biol 1998;10:572–577. [PubMed: 9818166]
26. Harden N. Signaling pathways directing the movement and fusion of epithelial sheets: lessons from dorsal closure in *Drosophila*. Differentiation 2002;70:181–203. [PubMed: 12147138]
27. Tepass U. Adherens junctions: new insight into assembly, modulation and function. Bioessays 2002;24:690–695. [PubMed: 12210528]
28. Bear JE, et al. Antagonism between Ena/VASP proteins and actin filament capping regulates fibroblast motility. Cell 2002;109:509–521. [PubMed: 12086607]
29. Kovacs EM, Ali RG, McCormack AJ, Yap AS. E-cadherin homophilic ligation directly signals through Rac and phosphatidylinositol 3-kinase to regulate adhesive contacts. J. Biol. Chem 2002;277:6708–6718. [PubMed: 11744701]
30. Sahai E, Marshall CJ. ROCK and Dia have opposing effects on adherens junctions downstream of Rho. Nature Cell Biol 2002;4:408–415. [PubMed: 11992112]
31. Vasioukhin V, Bauer C, Degenstein L, Wise B, Fuchs E. Hyperproliferation and defects in epithelial polarity upon conditional ablation of α-catenin in skin. Cell 2001;104:605–617. [PubMed: 11239416]
32. Huber O, Krohn M, Kemler R. A specific domain in α-catenin mediates binding to β-catenin or plakoglobin. J. Cell Sci 1997;110:1759–1765. [PubMed: 9264463]
33. Pokutta S, Weis WI. Structure of the dimerization and β-catenin-binding region of α-catenin. Mol. Cell 2000;5:533–543. [PubMed: 10882138]
34. Yang J, Dokurno P, Tonks NK, Barford D. Crystal structure of the M-fragment of α-catenin: implications for modulation of cell adhesion. EMBO J 2001;20:3645–3656. [PubMed: 11447106]
35. Pokutta S, Drees F, Takai Y, Nelson WJ, Weis WI. Biochemical and structural definition of the l-afadin- and actin-binding sites of α-catenin. J. Biol. Chem 2002;277:18868–18874. [PubMed: 11907041]

36. Woychik RP, Maas RL, Zeller R, Vogt TF, Leder P. 'Formins': proteins deduced from the alternative transcripts of the limb deformity gene. Nature 1990;346:850–853. [PubMed: 2392150]
37. Maas RL, Zeller R, Woychik RP, Vogt TF, Leder P. Disruption of formin-encoding transcripts in 2 mutant limb deformity alleles. Nature 1990;346:853–855. [PubMed: 2392151]
38. Wang CC, Chan DC, Leder P. The mouse formin (*Fmn*) gene: genomic structure, novel exons, and genetic mapping. Genomics 1997;39:303–311. [PubMed: 9119367]
39. Jackson-Grusby L, Kuo A, Leder P. A variant limb deformity transcript expressed in the embryonic mouse limb defines a novel formin. Genes Dev 1992;6:29–37. [PubMed: 1339380]
40. Caldwell JE, Heiss SG, Mermall V, Cooper JA. Effects of CapZ, an actin capping protein of muscle, on the polymerization of actin. Biochemistry 1989;28:8506–8514. [PubMed: 2557904]
41. MacLean-Fletcher S, Pollard TD. Mechanism of action of cytochalasin B on actin. Cell 1980;20:329–341. [PubMed: 6893016]
42. Khokha MK, Hsu D, Brunet LJ, Dionne MS, Harland RM. Gremlin is the BMP antagonist required for maintenance of Shh and Fgf signals during limb patterning. Nature Genet 2003;34:303–307. [PubMed: 12808456]
43. Nakano K, et al. Distinct actions and cooperative roles of ROCK and mDIa in Rho small G protein-induced reorganization of the actin cytoskeleton in Madin-Darby Canine Kidney cells. Mol. Biol. Cell 1999;10:2481–2491. [PubMed: 10436006]
44. Evangelista M, et al. Bni1p, a yeast formin linking cdc42p and the actin cytoskeleton during polarized morphogenesis. Science 1997;276:118–122. [PubMed: 9082982]
45. Imamura H, et al. Bni1p and Bnr1p: downstream targets of the Rho family small G-proteins which interact with profilin and regulate actin cytoskeleton in *Saccharomyces cerevisiae*. EMBO J 1997;16:2745–2755. [PubMed: 9184220]
46. Dong Y, Pruyne D, Bretscher A. Formin-dependent actin assembly is regulated by distinct modes of Rho signaling in yeast. J. Cell Biol 2003;161:1081–1092. [PubMed: 12810699]
47. Watanabe N, et al. p140mDia, a mammalian homolog of *Drosophila* diaphanous, is a target protein for Rho small GTPase and is a ligand for profilin. EMBO J 1997;16:3044–3056. [PubMed: 9214622]
48. Kohno H, et al. Bni1p implicated in cytoskeletal control is a putative target of Rho1p small GTP binding protein in *Saccharomyces cerevisiae*. EMBO J 1996;15:6060–6068. [PubMed: 8947028]
49. Alberts AS. Identification of a carboxyl-terminal diaphanous-related formin homology protein autoregulatory domain. J. Biol. Chem 2001;276:2824–2830. [PubMed: 11035012]
50. Perez-Moreno M, Jamora C, Fuchs E. Sticky business: orchestrating cellular signals at adherens junctions. Cell 2003;112:535–548. [PubMed: 12600316]

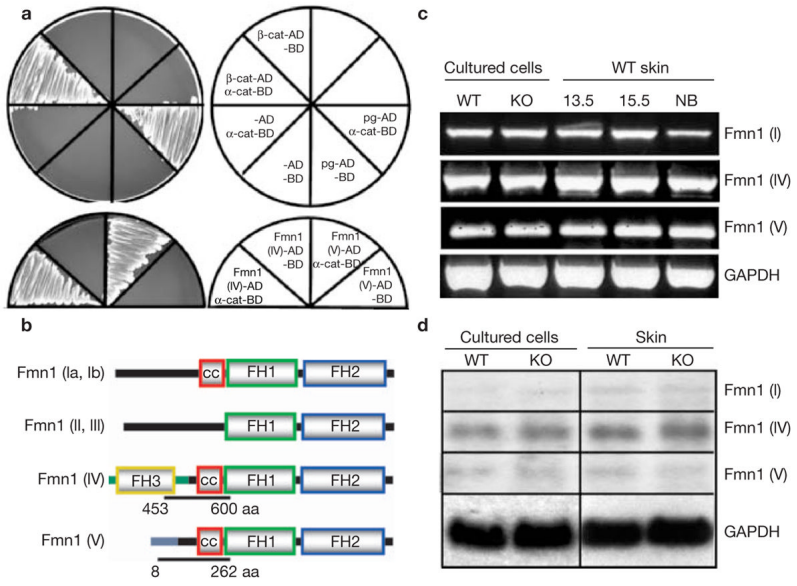

Figure 1.

Formin 1 is a putative interacting protein for α-catenin. (**a**) Full-length α-catenin linked to the Gal4 DNA-binding domain (BD) was used as bait to isolate proteins consisting of the Gal4 activating domain (AD) fused to sequences encoded by mouse skin cDNAs. Note specific interactions between α-catenin and two of its known interacting proteins, β-catenin (β-cat) and plakoglobin (pg), both of which were identified in the screen. Additionally, two clones encoding portions of formin-1 isoforms were identified: formin-1 (IV), a previously identified isoform, and formin-1 (V), a novel isoform. (**b**) A schematic representation of formin-1 isoforms. Formin-1 (Ia, Ib, II, III and IV) have been reported[38]. Formin-1 (V) was sequenced in its entirety. The sequences encoded by the two interacting clones are underlined, with their corresponding amino-acid residues indicated. FH, formin homology; cc, coiled-coil domain. (**c**) RT-PCR analysis to detect mRNAs encoding specific formin-1 isoforms in keratinocytes cultured from α-catenin conditional null (knockout) and wild-type mouse skin cultures, and *in vivo* skin from E13.5, E15.5 and newborn (NB) animals. GAPDH was used as a positive control. Bands specific for isoforms I, IV and V were detected and were of the predicted sizes. If at all present, mRNAs encoding isoforms II and III were expressed at levels below the limits of detection. (**d**) Northern blot analyses of the mRNA expression patterns of formin-1 isoforms in cultured keratinocytes and whole skin from wild-type and knockout mice.

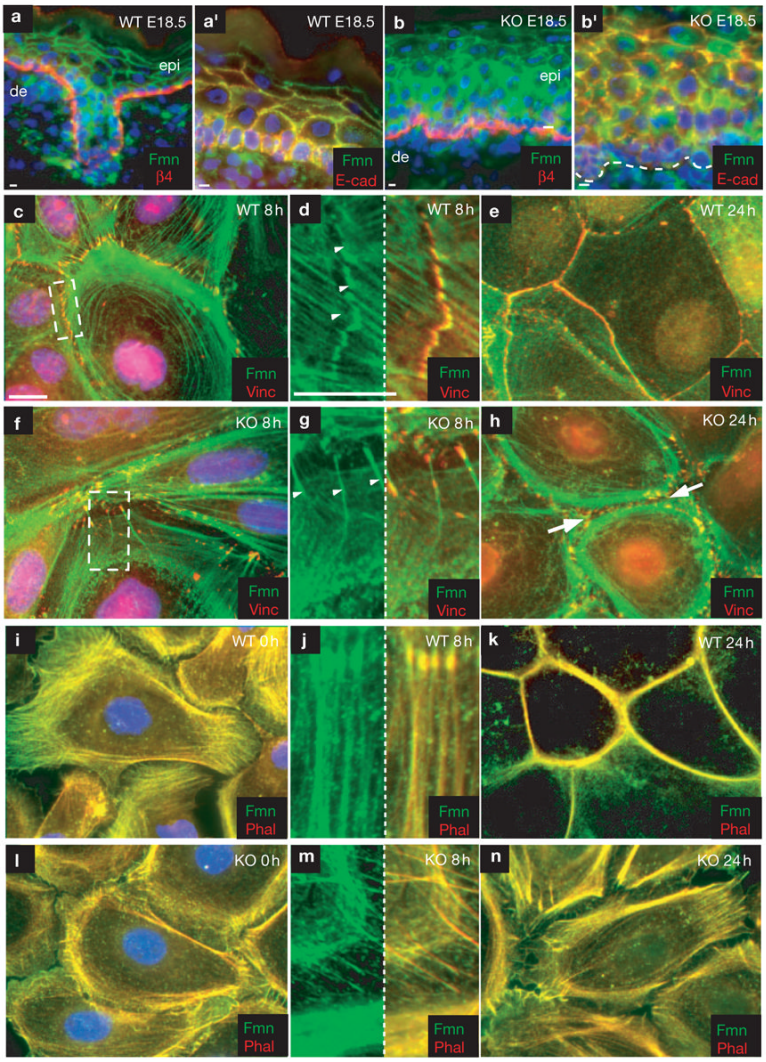

Figure 2.

The localization of Formin-1 is dependent on α-catenin. (**a**, **b**) Skin from wild-type and *α-catenin* knockout E18.5 mouse embryos were labelled with monospecific antibodies against formin-1 (IV) and either β4 integrin, to mark the epidermal (epi)–dermal (de) boundary (**a**, **b**), or E-cadherin, the transmembrane component of adherens junctions (**a′**, **b′**). Note cell–cell border staining in wild-type epidermis, but a more diffuse staining pattern in knockout epidermis. Some anti-formin-1 (IV) labelling was also detected in dermal cells. (**c**–**n**) Wild-type and *α-catenin*-null (KO) keratinocytes were cultured at high density overnight from the skins of newborn mice. At time zero, calcium was added to induce cell–cell adhesion, and at the times indicated thereafter. Cells were fixed before immunofluorescence staining with phalloidin, or antibodies against formin-1 (IV) or vinculin (Vinc), as indicated. After 8 h, adherens junctions are organized into distinctive rows of puncta (adhesion zippers), each with an associated radial cable of actin. After 24 h, an epithelial sheet has formed, with uniform adherens junction labelling at cell–cell borders. Note that formin-1 antibodies localize to puncta, radial actin cables and mature cell–cell borders. Note that formin-1 organization is perturbed in the absence of α-catenin, as are radial actin cables and adherens junctions. Notably, however, the overall actin cytoskeleton is largely intact in the knockout keratinocytes. Scale bars represent 10 μm.

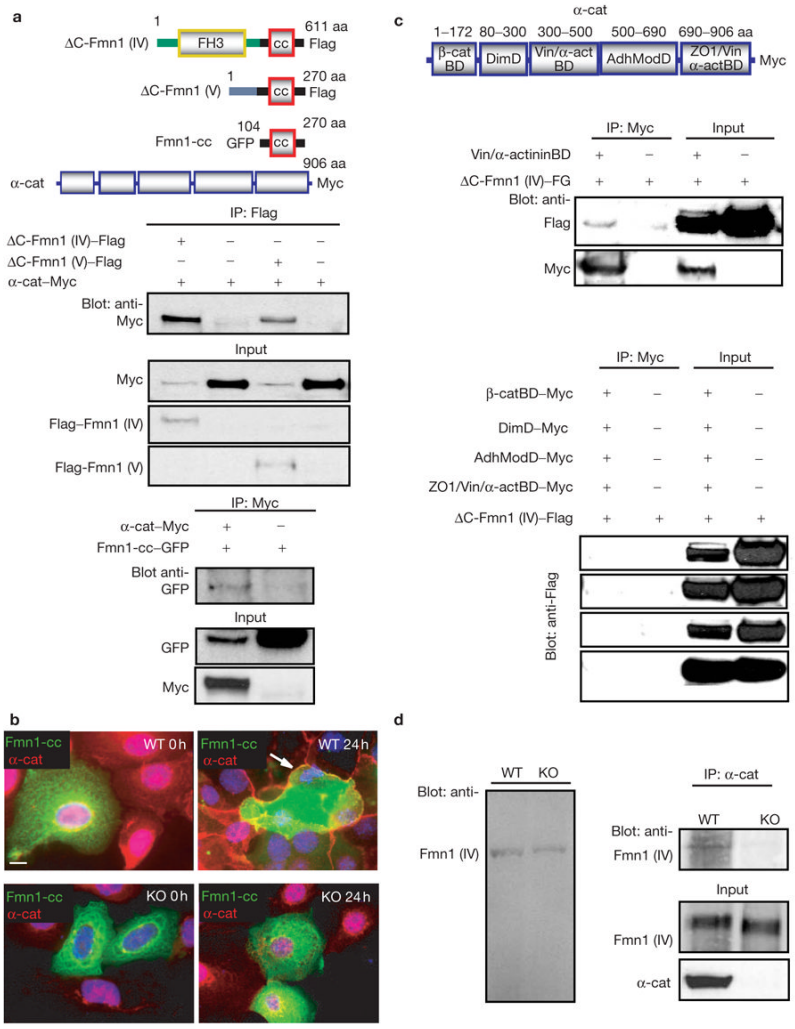

Figure 3.

Formin-1 and α-catenin interact specifically. (**a**) The top panel shows a schematic representation of Flag-tagged ΔC-formin-1 (IV) and ΔC-formin-1 (V), formin-1-cc (N-terminally GFP-tagged α-catenin-binding domain) and α-cat–Myc (full-length α-catenin with a C-terminal Myc tag). The middle panel shows CMV-driven expression of Flag-tagged ΔC-formin-1 (IV) and ΔC-formin-1 (V). The bottom panel shows CMV-driven expression of GFP-tagged formin-1-cc (142 amino acids). 48 h after transfection, protein extracts were subjected to immunoprecipitation (IP) with the indicated antibodies. Total protein lysates (input) and immunoprecipitated products were analysed by western blotting. Co-expressed transgenes were always expressed at reduced levels relative to singly expressed transgenes. (**b**) Wild-type and *α-catenin*-null (KO) keratinocytes expressing CMV-formin-1-cc were either treated with high levels of calcium (right panels) or left untreated (left panels). Cells were then analysed by indirect immunofluorescence microscopy. Scale bar denotes 10 μm. (**c**) The top panel shows a schematic representation of the structural domains of α-catenin[32-35]. β-cat-BD, β-catenin-binding domain; DimD, dimerization domain; Vin/α-actBD, vinculin- and α-actinin-binding domains; AdhModD, adhesion modulation domain; Z01/Vin/α-act-BD, Z01-, vinculin- and α-actinin-binding domains. Each domain was Myc-tagged and expressed transiently with ΔC-formin-1 (IV). Immunoprecipitation and western blotting were performed as in **a**. Only the vinculin/α-actinin domain of α-catenin associated specifically with ΔC-formin-1 (IV). (**d**)

Primary keratinocytes were lysed and subjected to anti-α-catenin immunoprecipitations. Samples were analysed by SDS–PAGE and western blotting with anti-formin-1 (IV) or anti-α catenin antibodies. Total lysates from wild-type and knockout keratinocytes were also subjected to anti-formin-1 (IV) western blotting.The formin-1 (IV) antibody is highly specific and detects a single band.

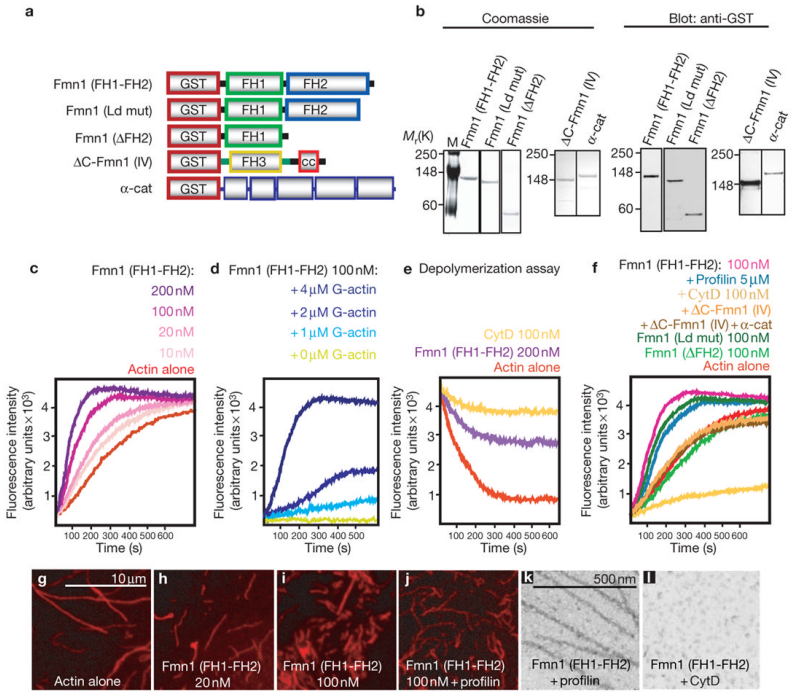

Figure 4.

Formin-1 (FH1-FH2) nucleates actin filaments *in vitro*. (**a**) A schematic representation of GST–formin-1 fusion proteins used for these studies. (**b**) Coomassie-blue-stained SDS–PAGE gels and anti-GST western blots of bacterially expressed and purified proteins. M, molecular markers. (**c**) Nucleation of actin filaments by domains of formin-1, as determined by the pyrene–actin assembly assay. Assembly reactions contained 4 μM actin (10% pyrene actin) and formin-1 (FH1-FH2) between 10 and 200 nM. (**d**) Assembly reactions were performed as in **c**, except that the formin-1 (FH1-FH2) concentration was maintained at 100 nM and the actin concentration varied between 0 and 4 μM. (**e**) Time course of depolymerization of 5 μM actin filaments (10% pyrene-labelled) after dilution to 0.1 μM in the presence of 200 nM formin-1 (FH1-FH2), cytochalasin D (CytD), or actin alone, as indicated. (**f**) The effects of profilin, cytochalasin D, *ld/ld* truncation (Ld mut), removal of the FH2 domain (ΔFH2), ΔC-formin-1 and α-catenin on formin-1-induced actin polymerization. The formin-1 fragments in **a** were added to 4 μM pyrene–actin and filament assembly was monitored. For formin-1 (FH1-FH2) reactions were also conducted in the presence or absence of 5 μM profilin or 100 nM cytochalasin D. (**g**–**j**) Epifluorescence imaging of aliquots of select assembly reactions from **c**–**f** as indicated. (**k**) Electron micrograph of assembly reaction containing 100 nM formin-1 (FH1-FH2), 4 μM actin (10% pyrene–actin) and 5 μM profilin. (**l**) The same reaction as in **k** performed in the presence of cytochalasin D.

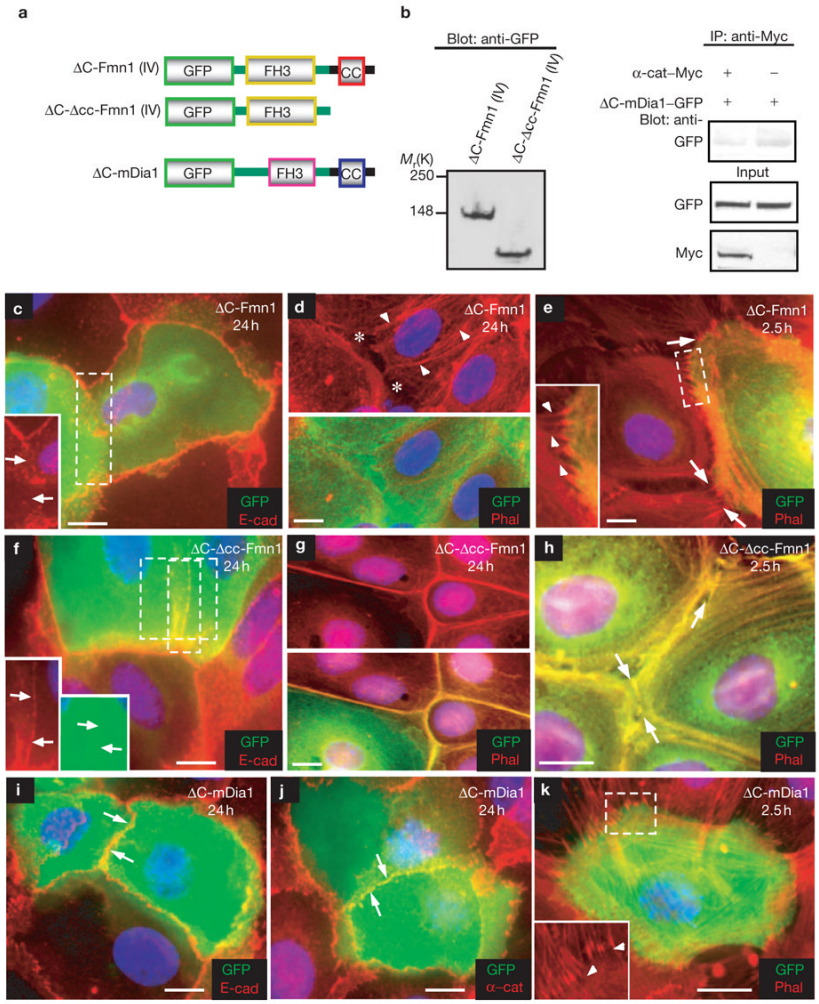

Figure 5.

The formin-1 α-cat-BD perturbs intercellular junctions. (**a**) A schematic representation of the GFP fusion proteins used in this study. (**b**) The left panels shows an anti-GFP western blot to verify the size and stable expression of the proteins. The right panel shows immunoprecipitations, demonstrating that ΔC-mDia1, the mDia1 equivalent of ΔC-formin-1 (IV), does not bind to α-catenin. (**c**–**k**) Transient expression of ΔC-formin-1 (IV) (**c**–**e**), ΔC-Δcc-formin-1 (IV) (**f**–**h**) or ΔC-mDia1 (**i**–**k**) in primary, wild-type, keratinocytes. High-calcium medium was added 24 h after transfection. After a further 2.5 or 24 h, cells were analysed by indirect immunofluorescence microscopy with the indicated antibodies or with rhodamine–phalloidin. Boxed areas are shown at higher magnification in insets. Opposing arrows in **c** and asterisks in **d** denote disruption of cell–cell junctions between two cells transfected with ΔC-formin-1. Arrows and arrowheads in **e** depict puncta-associated radial actin cables present only in untransfected cells and not in transfected cells. Opposing arrows in **f**–**k** denote cell–cell junctions between two cells transfected with ΔC-Δcc-formin-1 or ΔC-mDia1. Arrowheads in **k** denote radial actin cables still present in a ΔC-mDia1-transfected cell. Scale bars in **c**–**k** represent 10 μm.

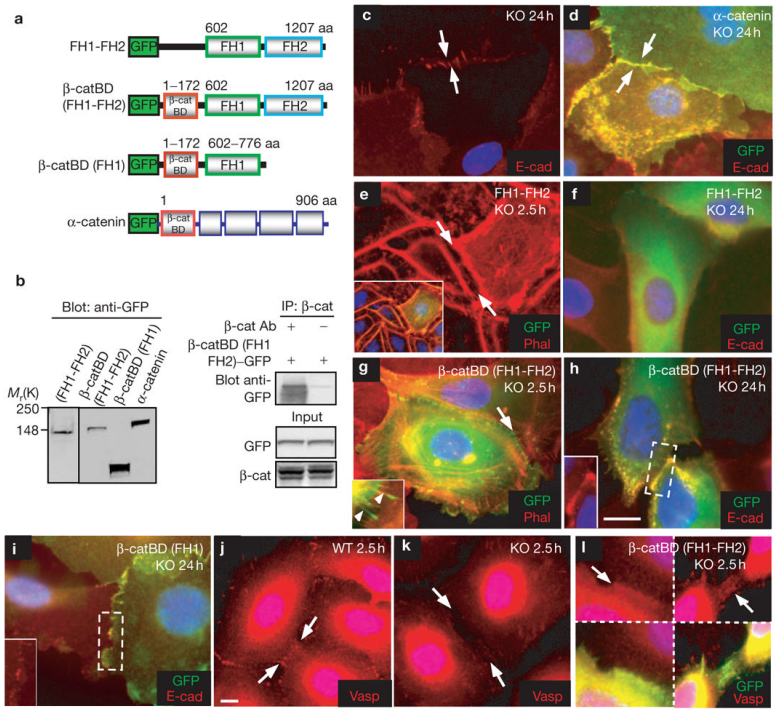

Figure 6.

Rescuing intercellular junctions in *α-catenin*-null keratinocytes. (**a**) A schematic representation of the GFP fusion proteins used in this study. (**b**) Western blot and co-immunoprecipitation analyses, as described in Fig. 1, showing that the proteins are stably expressed and of the predicted sizes, and that they associate with β-catenin. (**c**–**l**) Rescue experiments. *α-catenin*-null (KO) keratinocytes were transfected as indicated in low-calcium medium. After 24 h, cultures were shifted to high-calcium medium for the indicated times before analysis by indirect immunofluorescence microscopy. The antibodies used are indicated. Arrows in **c** and **d** denote cell–cell borders. The cell borders in **c**, **e**, **f** and **i** lack proper adherens junctions. Scale bars in **c**–**l** represent 10 μm.